Eur. Phys. J. B (2015) 88: 248
DOI: 10.1140/epjb/e2015-60001-2

THE EUROPEAN PHYSICAL JOURNAL B

Regular Article

Study of the electronic structure of Ag, Au, Pt and Pd clusters adsorption on graphene and their effect on conductivity

Roxana Mitzayé Del Castillo and Luis Enrique Sansores[a]

Instituto de Investigaciones en Materiales, Universidad Nacional Autónoma de México, Circuito Exterior s/n, Apartado Postal 70-360, C.P. 04510, México, D.F., Mexico

Received 2 January 2015 / Received in final form 9 June 2015
Published online 7 October 2015 –

Abstract. When metallic clusters are adsorbed by pristine graphene, the conductivity of the system is modified. In this paper the adsorption of silver, gold, platinum and palladium cluster with n atoms ($n = 1$, 2, 3 and 4) and their effect on conductivity are studied. Ground state properties and electronic structure calculations at DFT level are undertaken for each system. Conductivity is calculated taking three different approaches; frozen ripples, charged impurities and resonant scattering. Adsorption sites are the scattering centres of our systems. For conductivity calculations, size and scattering potential are obtained from our calculations. Systems Pt and Pd are in the chemisorption range and the network distortion is such that conductivity diminishes so that it is no longer in the ballistic regimen. Systems Ag and Au are in the physisorption range, the network preserves the natural two dimensionality of the graphene sheet and conductivity is still in the ballistic regimen.

1 Introduction

From the time graphene was produced by applying a procedure of micromechanical cleavage to graphite [1], many interesting applications using its physical properties have been revealed. In particular, it has been identified as an alternative to indium tin oxide (ITO), in transparent conductive electrodes [2], which are critical components of optoelectronic devices such as touch panels [3,4], sensors [5] and solar cells [6]. The main problem facing the industrial sector is to create electrodes with low sheet resistance and effective light transmittance. The experimental group headed by Bae report a 30-inch graphene monolayer with a sheet resistance as low as 125 $\Omega\,\mathrm{sq}^{-1}$, manifesting 97.4% optical transmittance [2].

Graphene shows a linear dispersion relationship for the electronic band in k-space, such that the electrons behave like Fermi-Dirac fermions. The effective velocity of these electrons is approximately 10^6 m/s [7], hence, graphene manifests ballistic conductivity. This implies that electrons have negligible electrical resistivity caused by scattering. Experimentally, it has been found that graphene conductivity depends slightly on temperature and is approximately proportional to carrier concentration n; the electron mobility in graphene is about 15 000 $\mathrm{cm}^2/\mathrm{V\,s}$ [8]. Thus, mathematical explanations include the hypothesis that interactions of scattering centres should be long range. The most commonly used approach considers the charged impurities as Coulombic centres [9]. However, some experimental data cannot be described with this approximation, as electron mobility depends on dielectric screening on a small-scale. There are alternative explanations for describing the scattering mechanism, such as frozen ripples [10], charged impurities [11] and resonant scattering [12]. Following the frozen ripples approach, the long-range character of the interactions is due to elastic deformations and impurities provide another source of static disorders, manifesting as a corrugation in the network. The charged impurities have a cross section proportional to k_{F}^{-1}, and a long-range scattering potential. The scattering phases for massless Dirac fermions are energy independent to n. Likewise the resonant scattering approach focuses on the use of an additional scattering mechanism involving midgap states, leading to a similar k dependence on relaxation time as charged impurities.

It is generally well-known that cluster formation of different metals on graphene can take place in a stable way. Also notably, molecules such as NO_2, NH_2 and H_2O can be adsorbed at room temperature [13]; in contrast to the adsorption of these molecules on graphite, where adsorption only occurs below liquid-nitrogen temperatures [14]. Mc Creary et al. [15] investigated the effect of gold atoms and clusters on the transport properties of graphene. They made a cryogenic deposition (18 K) of Au, subsequently increasing the temperature to room temperature in order to promote cluster formation, and finally conductivity was measured. They concluded that Au cluster formation increases mobility, whereas a homogeneous distribution reduces it. Tien et al. reported aggregation and restacking graphene nanosheets decorated with silver nanoparticles,

[a] e-mail: sansores@unam.mx

with a maximum sheet resistance of 93 Ω sq^{-1} and a 78% light transmittance providing another way of obtaining transparent conductive films [16].

Vanin et al. [17] studied the adsorption of Co, Ni, Pd, Ag, Au, Cu and Pt single atoms on pristine graphene by LDA and vdW-DF. They revealed strong binding for Co, Ni and Pd, whereas Ag, Au, Cu and Pt show weak binding on graphene. Amft et al. [18] focused on the Van der Waals interactions of Cu, Ag and Au single atoms on graphene. They compared vdW-DF and PBE + D2 methods and found out that this metal atom binds weakly on graphene sheets, demonstrating that Van der Waals interactions represent the most important forces on these systems. Cabria et al. [19] studied the interaction of palladium clusters on graphene and discerned that three-dimensional clusters are more stable than planar clusters. The transition from planar to three-dimensional structures occurs as a consequence of the Pd-Pd interaction.

The main aim of this paper is to study the effect of adsorption of small metallic clusters supported on graphene sheets and to observe the extent of change in conductivity. We also study how clustering of adsorbates can influence the electronic properties of graphene. We calculate conductivity using these approximations: frozen ripples [10], charged impurity scattering [11] and resonant scattering approaches [12]. The metallic clusters M_n were formed with n atoms (n = 1, 2, 3 and 4) of M = Ag, Au, Pt or Pd.

2 Methodology

Graphene sheets were modelled by applying a 6×6 supercell approach (72 carbon atoms), using the calculated C-C bond length of 1.42 Å. The z-axis of the periodic supercell was large enough (30 Å) to ensure that the interaction between two successive layers was negligible.

Ground-state structures, adsorption energies, Löwdin charges and density of states (DOS) have been calculated, using the plane-wave pseudo-potential method implemented in the QUANTUM ESPRESSO computational package [20]. Density Functional Theory (DFT) calculations were performed using a plane wave basis set and pseudopotentials. The exchange-correlation interaction was treated in the generalized gradient approximation (GGA), applying the Perdew-Burke-Ernzerhof parameterization (PBE) [21]. Kohn-Sham orbitals were expanded in a plane-wave basis-set up to a kinetic energy cutoff of 40 Ry. Self-consistent calculations for the Kohn-Sham equations were carried out by employing the convergence criterion of 10^{-8} Ry. Brillouin-zone integrations have been performed by applying the Methfessel-Paxton smearing special-point technique [22], using a smearing parameter of 0.05 Ry. The k-point selection was made based on Monkhorst-Pack [23] G-centred $4 \times 4 \times 1$ k-point mesh. The pseudopotentials for C, Ag, Au, Pt and Pd were chosen from the quantum espresso website[1], applying the Vanderbilt approach [24]. For metals, we have selected those whose distinguishing feature is being scalar relativistic ultrasoft with a nonlinear core correction. The pseudo-potential for Ag and Pd uses a Kr-like core, whereas Au and Pt use a Xe-like core. The generation of smooth pseudo-orbitals from atomic all-electron orbitals was made using the popular method: Rappe-Rabe-Kaxiras-Joannopoulos (RRKJ) [25].

The initial positioning for all graphene-cluster systems consisted of placing a metallic cluster over one carbon (Top-site position) or between two carbon atoms (Bridge site), right in the middle of the graphene sheet, at a distance of 3.0 Å. For the dimer case (graphene-Ag_2, graphene-Au_2, graphene-Pt_2 and graphene-Pd_2) two possible initial positions were studied: horizontal line (the two metallic atoms on the graphene sheet at the same height) and vertical line (carbon-metallic atom-metallic atom were aligned, resulting in a straight vertical line). The trimer case (graphene-Ag_3, graphene-Au_3, graphene-Pt_3 and graphene-Pd_3) has four possible configurations; horizontal line, vertical line, horizontal triangle (the three metallic atoms form a horizontal triangle over the graphene sheet and are at the same height) and vertical triangle (two metallic atoms which form the triangle base are at the same height of two adjacent Carbons). The tetramer has been designed for nine initial configurations: horizontal and vertical line, a rhombohedral isomer (Diamond-shape) in horizontal and vertical position, with acute vertex pointing down and parallel to graphene plane (n); a planar triangle plus an extra metallic atom (Y-shape) in horizontal, vertical position with vertex pointing up and vertex parallel to graphene plane (n); and a tetrahedral isomer (three atoms are close to the graphene sheet).

The adsorption energy has been calculated according to the formula

$$E_a = E\,(\text{graphene} + \text{M}_n) - [E\,(\text{graphene}) + E\,(\text{M}_n)],$$

which is used as the measure for stability in the systems studied. The $E(\text{M}_n)$ and E(graphene) are the energies of the free metallic cluster optimised in vacuum and the graphene layer respectively and $E(\text{graphene} + \text{M}_n)$ is the energy of the system formed by the cluster adsorbed on graphene sheet, optimised using the same methodology. Negative adsorption energy indicates that adsorption is exothermic.

3 Results

3.1 Ground-state properties. Adsorption sites and adsorption energies

Following geometry optimisation, the bond lengths of each graphene-M_1 system were measured and compared with

[1] Ultrasoft pseudopotentials for C, Ag, Au, Pd and Pt were taken from the Pwscf PseudoPotential Download Page http://www.quantum-espresso.org (Files: C.pbe-van_ak.UP, Ag.pbe-d-rrkjus.UPF, Au.pbe-nd-rrkjus.UPF, Pt.pbe-nd-rrkjus.UPF and Pd.pbe-n-rrkjus_psl.0.2.2.UPF).

Table 1. Optimised geometry data and adsorption energies of Ag, Au, Pt and Pd clusters supported on graphene. Distances (d) in Å, adsorption energies (E_a) in eV and n is the number of atoms in the clusters. For systems with one metallic atom we show the comparison between metal-carbon bond lengths (Å) obtained in this work and results in the scientific literature.

Graphene-M$_n$	n	$d_{\text{M-C}}$//Other results (Method)	$d_{\text{M-M}}$	E_a	Geometry
Graphene-Ag$_n$	1	3.26//3.30 (vdW-DF) [18]		–0.027	Top-site
	2	2.63	2.58	–0.125	Vertical line
	3	2.49 2.52	2.78 2.70 2.66	–0.358	Vertical triangle Y-shape
	4	2.48	2.61 2.63 2.76(2)	–0.297	Vertical 1
Graphene-Au$_n$	1	2.61//2.65 (vdW-DF) [18]		–0.310	Top-site
	2	2.32	2.53	–0.640	Vertical line
	3	2.34 2.35	2.65(2) 2.75	–0.754	Vertical Triangle
	4	2.32	2.55 2.61 2.67 2.70	–0.663	Y-shape Vertical 1
Graphene-Pt$_n$	1	2.09 2.10//2.08 (PBE-Vanderbilt) [26]		–1.196	Bridge-site
	2	2.23 2.22	2.41	–0.943	Vertical line
	3	2.17 2.23	2.53(2) 2.59	–1.816	Vertical Triangle
	4	2.17 2.25	2.53 2.65(2) 2.66(3)	–1.274	Tetrahedral
Graphene-Pd$_n$	1	2.13 2.15//2.14 (GGA-PW91) [19]		–1.203	Bridge-site
	2	2.13 2.23	2.70	–1.348	Vertical Line
	3	2.26(4)	2.46 2.55(2)	–1.977	Vertical Triangle
	4	2.19	2.55 2.57(2) 2.62 2.66(2)	–0.611	Tetrahedral

previously reported results. As shown in Table 1, the results are very similar to those found in previous studies. In Figure 1, ground state geometries obtained after geometry optimisations are presented. In Table 1, the distances between the cluster and the nearest carbon on the sheet, and the distances between the atoms forming the clusters and their adsorption energies for each ground state system are displayed.

Graphene-Ag$_1$ and graphene-Au$_1$ systems have a final adsorption site on top of a carbon atom pertaining to the graphene sheet (Top-site), which is consistent with previous studies made by Amft et al. [18]. The bond length of graphene-Ag$_1$ is 3.26 Å and graphene-Au$_1$ is 2.61 Å. Meanwhile, Amft's group obtained a bond length on graphene-Ag$_1$ of 3.30 Å and graphene-Au$_1$ of 2.65 Å (see Tab. 1). Following geometry optimisation, it appears that every single horizontal structure tends to become a vertical structure standing perpendicular to the graphene plane. For graphene-Ag$_2$ and graphene-Au$_2$ systems, the ground state represents a line standing perpendicular to the graphene sheet as shown in Figure 1, the position of the vertical line is Top-site with an adsorption energy of –0.125 eV for graphene-Ag$_2$ and –0.640 eV for graphene-Au$_2$, which means that they both comply with the physisorption scheme. The ground state of systems graphene-Ag$_3$ and graphene-Au$_3$ is a vertical triangle with the apex down (∇) shown in Figure 1, the apex is just above the C-C bond (Bridge-site) with a bond length of 2.49 Å for graphene-Ag$_3$ and 2.34 Å for graphene-Au$_3$. For graphene-Ag$_4$and graphene-Au$_4$ the

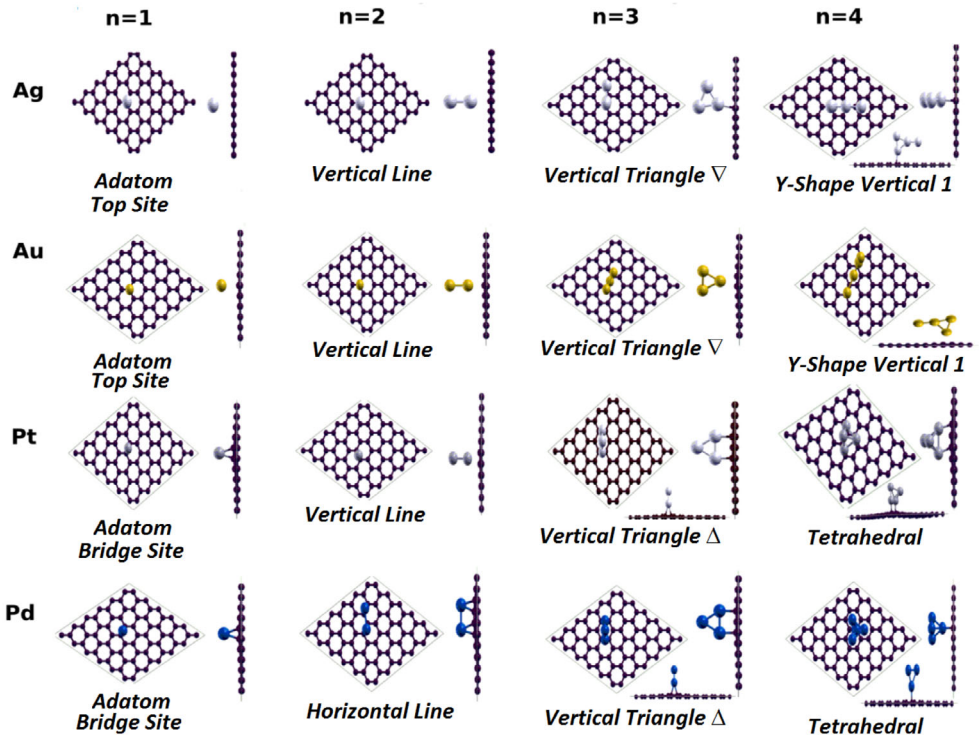

Fig. 1. Ground-state structures of graphene-Ag_{1-4}, graphene-Au_{1-4}, graphene-Pt_{1-4} and graphene-Pd_{1-4}. These are optimised geometries.

ground state is Y-shape in vertical position with vertex parallel to the graphene plane; these are shown in Figure 1. Studies made by Grönbeck and Andreoni with a level of theory DFT-BLYP show that tetrahedral structure of Au_4 is unstable in gas phase and the ground state is a diamond-shaped isomer [27]. Indeed, following geometry optimisation, the tetrahedral isomer on graphene becomes a diamond-shape vertical isomer [28], with higher energy than the Y-shape vertical isomer, concurring with other studies. The same occurs with graphene-Ag_4, with the difference that the tetrahedral isomer is stable in gas phase. All adsorption energies for graphene-Ag_{1-4} and graphene-Au_{1-4} are in the range of physisorption. The bond length indicates to us that Ag-Ag, Au-Au interactions are stronger than Ag-C, and Au-C interactions.

After geometry optimisation of graphene-Pt_1 system, the adsorption position was the Bridge-site (Fig. 1). The bond length obtained between Pt-C is 2.09 Å, concurring with Okazaki-Maeda's group [26]. They obtained a bond length of 2.08 Å using a PBE method and taking a Vanderbilt pseudopotential approach, as shown in Table 1. For the graphene-Pt_2 system, it is possible to have two configurations: the horizontal line and the vertical line. The most stable configuration is the vertical line in Bridge-site, with adsorption energy of –0.943 eV (Fig. 1). The graphene-Pt_3 system has four possible configurations: the horizontal line, vertical line, horizontal triangle and vertical triangle. According to the adsorption energy (–1.816 eV), the most stable configuration is the trimer with the vertical triangle shape, with the apex up (Δ) on Bridge-site, i.e. each Pt of the base is at the mid-point of a C-C bond. In a theoretical study undertaken by Grönbeck and Andreoni [27], they studied the Pt_{2-5} clusters alone and realized that the triangle isomer is more stable than the linear isomer. We obtain the same result in the graphene-Pt_3 interaction (Fig. 1). For tetramer configurations, the most stable one is the tetrahedral isomer with adsorption energy of –1.274 eV, suggesting chemisorption. Meanwhile Grönbeck and Andreoni observed that the ground state for the tetramer alone in gas phase is the Y-shape [27]. The stable structures are those that are tridimensional, it is inferred that the number of platinum atoms binding to graphene are reduced to minimum.

For graphene-Pd_1 systems, following geometry optimisation, the Bridge-site represented the final position. The Pd-C bond length was found at 2.15 Å according to results published by Thapa et al. (2.17 Å), using a PBE method and a Vanderbilt ultrasoft pseudopotential approach [29] and also with the results obtained by Cabria et al. (2.14 Å) at theory level GGA-PW91 [19], shown in Table 1. Graphene-Pd_2 system has two possible configurations; the horizontal dimer and the vertical dimer. The horizontal dimer is the most stable structure with adsorption energy of –1.348 eV, with each palladium in Bridge-site position (Fig. 1). The big surprise comes in the case of the graphene-Pd_3 system, where only two configurations are available; the horizontal triangle and the vertical triangle. The horizontal line and vertical line are unstable and they turn into horizontal and vertical triangles, respectively. The ground state is the apex-up vertical triangle configuration (Δ), each Pd is in Bridge-site position, and

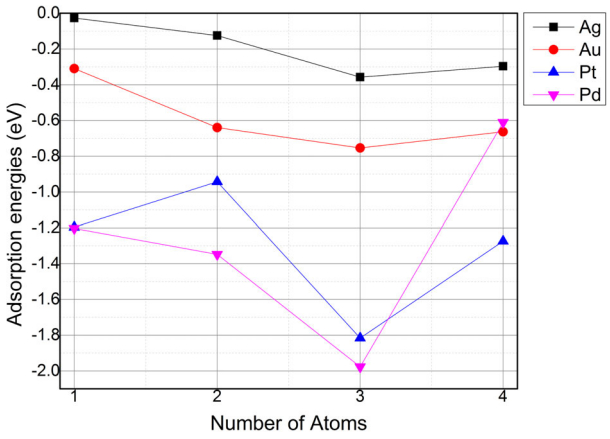

Fig. 2. Number of Atoms vs. adsorption energies for ground-state geometries.

the adsorption energy is –1.977 eV. Likewise, the tetramer configuration is a very interesting case, with only one stable configuration; the tetrahedral isomer with an adsorption energy of –0.612 eV. The Pd-Pd bond length in the system graphene-Pd_n is larger than the bond length of the cluster in vacuum due to the influence of the graphene substrate. In our calculations, the isolated Pd_2 has a bond length of 2.39 Å, Pd_2 on graphene has a bond length of 2.54 Å, and the experimental case of Pd_2 on graphene was reported as 2.57 Å [30]. We can see that all adsorption energies for this system relate to the chemisorption range. Graphene-Pd_{1-4} systems prefer tridimensional structures. This indicates that Pd-Pd interaction is stronger than Pd-C, just as in the Pt case.

Comparing the adsorption energy, the adsorption sites and bond length, the most stable system is the trimer cluster on graphene (Fig. 2). This stability depends on the covalent atomic radius; the adsorption site (Top-sites are less stable than Bridge-sites, suggesting that smaller atoms can be accommodated between C-C bonds) and the distortion of the network (as distortion increases stability increases, too). It would be more energetically favourable for the metallic atoms to stick together, and form a vertical triangle, than separate from each other onto the surface. For graphene-Pd_4 system, the tetrahedral isomer does not fit in C-C bonds and rotates so that that the tip ends up in Top-site, thus destabilising the metallic-graphene array.

3.2 Electronic structure

In this section, we discuss the mechanism for molecular adsorption and conductivity as the standpoint for density of states (DOS) and charge transfer. Following the results found by Leenaerts et al. [31], we can describe two charge transfer mechanisms in terms of the highest occupied molecular orbital (HOMO) and the lowest unoccupied molecular orbital (LUMO) of the adsorbate; these are visible as peaks in the DOS: (i) If the HOMO exceeds the Fermi level of pure graphene, i.e. the Dirac point, there is a charge transfer from the cluster to the graphene. If the LUMO falls below the Dirac point, the charge will transfer from the graphene to the cluster. (ii) The charge transfer between the cluster and graphene is also partially determined by the mixing of the HOMO and LUMO, with the graphene's orbital due to hybridization. The Lödwin population analysis [32] of the ground-state structures (Tab. 2) is also presented.

Figure 3 shows the DOS of the ground state configurations for graphene-Ag_{1-4} systems in comparison with pure graphene (black line), the ideal DOS for pure graphene is characterized by two main properties; it has a linear dependence in energy around the Dirac point and there are two Van Hove singularities near ±G [33]. When adsorbates are introduced in the system, the Fermi level is shifted away from the Dirac point and the van Hove singularities are steadily broadened with respect to the adsorbate density. The electronic configuration for the silver atom is [Kr] $4d^{10}\ 5s^1$, so that silver contributes to DOS with the $4d$ and $5s$ orbitals. In the DOS of graphene-Ag_1 system, there is a big peak in the occupied orbitals region (E_g), which is a superposition of $4d$ orbitals of silver and $1p$ orbital of the nearest carbon. The Fermi energy is at midpoint of the HOMO (A_{1g}) orbital of the Ag and is completely affected by the $5s$ orbital of silver. In this case, the HOMO is above the Dirac point and the charge transfer occurs from the Ag atom to the graphene sheet. The Lödwin analysis shows the same result, as charge transfer occurs weakly from the silver atom to the graphene surface, i.e the Ag atom will act as a donor (p-type). In the case of the graphene-Ag_2 system, the peaks π_g and σ_u are a superposition of the $4d$ orbital of silver atoms of dimer and the $1p$ orbital of the nearest carbon. The HOMO orbitals (σ_u) is affected by the $5s$ orbital of the nearest silver to graphene surface, meanwhile the LUMO orbital (π_u) is affected by the $5s$ orbital of the silver atom, which is farthest from the graphene surface. The region near the Fermi energy is affected very weakly by the cluster, the occupied and unoccupied electronic states of this system are separately by Hund exchange energy of the order of 1.5 eV. The Lödwin analysis shows that the charge transfer occurs from the silver nearest to the graphene surface, towards the farthest silver and towards the graphene surface.

In the graphene-Ag_3 system, DOS has to the peaks (1A′) and (1A″), with main contributions from the $4d$ orbitals of the silver trimer and the $1p$ orbitals of the 3 nearest carbons. The LUMO orbital contributions (3A′) are the superposition of the $5s$ orbitals of the silver trimer and do not greatly affect the Fermi energy region. The Lödwin analysis shows that the charge transfer occurs from two silvers of the trimer to the other silver and to the graphene sheet, a system known as p-type doping. In the graphene-Ag_4 system, the DOS presents an increment of density of states in the region affected directly by the tetramer. The peaks (1A), (2A) and (3A) in the occupied state region receive contributions from the $4d$ orbitals of the silver tetramer and the $1p$ orbital of the nearest carbons. The Fermi energy region has a contribution of one $5s$ orbital from the nearest silver, the other $5s$ orbitals affect the LUMO (4A) orbital of tetramer and the state 5A. The Fermi energy is higher than the Dirac point, making

Table 2. Lödwin population analysis for each cluster and first neighbour carbons. ΔQ is the difference between total charge before and after adsorption. Only the nearest neighbour charges to the cluster are shown. In many cases, the opposite sign charges are distant from the point of interest, so the sum is not zero.

	$n=1$		$n=2$		$n=3$		$n=4$	
								ΔQ
				ΔQ		ΔQ	Ag	0.4207
					Ag	0.4154	Ag	0.2714
		ΔQ	Ag	0.1215	Ag	–0.0212	Ag	–0.208
Ag					Ag	0.0205	Ag	–0.2075
	Ag	0.0048	Ag	–0.0854	C	–0.038	C	0.0406
					C	–0.0097	C	–0.0268
	C	0.0287	C	–0.0095	C	0.027	C	0.0247
					C	0.0185	C	0.02
				ΔQ		ΔQ		ΔQ
					Au	–0.0432	Au	0.0474
		ΔQ	Au	–0.1084	Au	–0.0468	Au	0.071
Au					Au	0.0078	Au	–0.2806
	Au	–0.2462	Au	–0.1565	C	0.0122	Au	–0.1091
					C	0.0122	C	0.0136
	C	0.0431	C	0.0109	C	0.0463	C	0.0556
							C	0.0556
				ΔQ		ΔQ		ΔQ
					Pt	0.2534	Pt	0.2883
		ΔQ	Pt	0.17	Pt	0.2257	Pt	0.2811
					Pt	–0.2304	Pt	0.0075
Pt	Pt	0.0924	Pt	–0.22	C	–0.0119	Pt	–0.1153
					C	–0.0221	C	–0.0305
	C	0.0086	C	–0.02	C	–0.0265	C	–0.0109
					C	–0.016	C	–0.0027
	C	0.0083	C	–0.02			C	0.0269
				ΔQ		ΔQ		ΔQ
					Pd	–0.04	Pd	0.005
		ΔQ	Pd	0.0082	Pd	–0.04	Pd	0.0051
					Pd	–0.04	Pd	–0.0747
Pd	Pd	0.0243	Pd	0.0082	C	0.04	Pd	0.0052
					C	0.04	C	0.0266
	C	0.036	C	0.0319	C	0.04	C	0.0311
					C	0.04	C	0.0326
	C	0.0361	C	0.0319	C	0.04	C	0.033
					C	0.04		

a p-type doping system. The Lödwin analysis indicates that the charge transfer takes place from two silvers to the other two silvers and to the graphene surface. This charge transfer is reflected in the $5s$ orbitals of silver and $1p$ orbitals of carbon. The graphene-Ag_n systems generate p-type doping.

Figure 4 shows the DOS of the ground state configurations for graphene-Au_{1-4} systems in comparison with pure graphene (black line). The electronic configuration for gold atom is [Xe] $4f^{14}\ 5d^{10}\ 6s^1$, making contributions to DOS with $5d$ and $6s$ orbitals. In graphene-Au_1 system, the HOMO (T_{2g}) orbital of Au represents a superposition of the $5d$ orbitals of the gold atom and the $1p$ orbital on the nearest carbon. The LUMO (A_{1g}) orbital is completely due to $6s$ orbital of the gold atom. The Fermi energy of the full system and LUMO of Au are below the Dirac point, so the charge transfer is from the graphene sheet to Au. Lödwin charge analysis shows that charge transfer occurs from the graphene surface to the gold atom, partially filling the $6p$ orbital, evident in the DOS as a brown line in the virtual region. In the graphene-Au_2 system, the peak, π_g represents a superposition of the $5d$ orbital of both gold atoms of the dimer and $1p$ orbital of nearest carbon. Next peak, π_g is a superposition of the $6s$ orbital of gold and $1p$ orbital of carbon. The HOMO (σ_u) orbital is has contributions from $5d$ orbital and $6s$ orbital of the gold atom and $1p$ of the carbon. Peak π_u in the virtual region is mainly due to a $6p$ orbital of gold. The Lödwin charge analysis shows that charge transfer occurs from the graphene sheet to the gold atom, partially filling the $6p$ orbital. In graphene-Au_3 system, DOS has peaks ($2A'$) and ($1A''$) representing the sum of $5d$ orbitals of the trimer and $1p$ orbital of carbon. Peak ($3A'$) and the HOMO ($4A'$) orbital include the contribution of $5d$ orbitals and $6s$ orbitals of the trimer and $1p$ orbital of the 3 nearest carbons. The LUMO ($5A'$) orbital also has a contribution of $6s$ of the trimer and $1p$ orbital of graphene sheet carbons. Lödwin charge analysis shows that the charge transfer occurs from

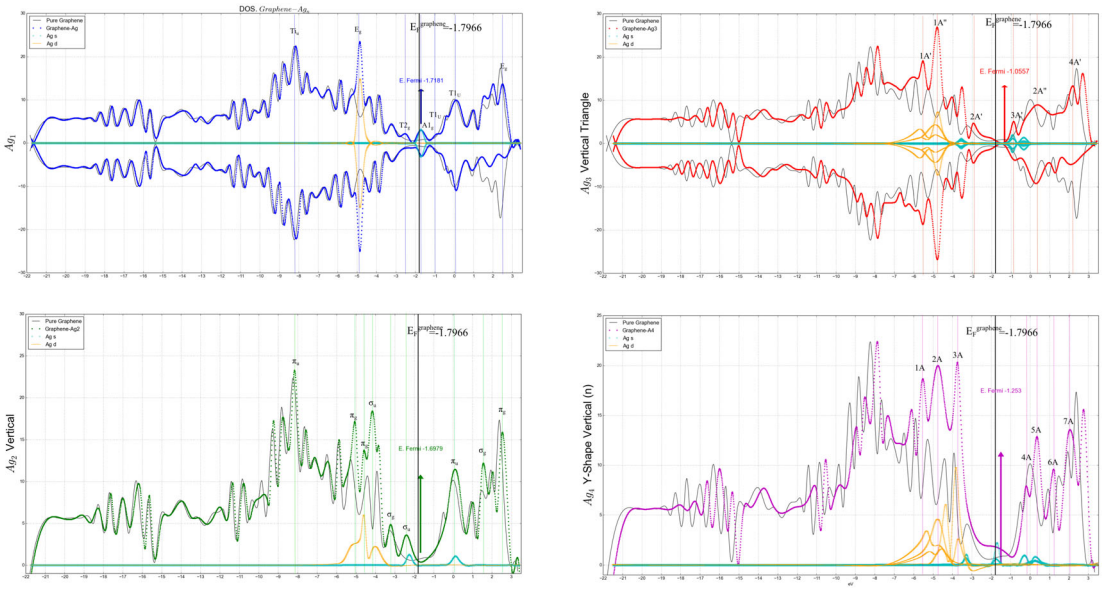

Fig. 3. DOS of graphene-Ag_n system. Pure graphene (black line); the Fermi energy for pure graphene is –1.797 eV; contributions of the MOs of Ag_n are indicated with dotted lines.

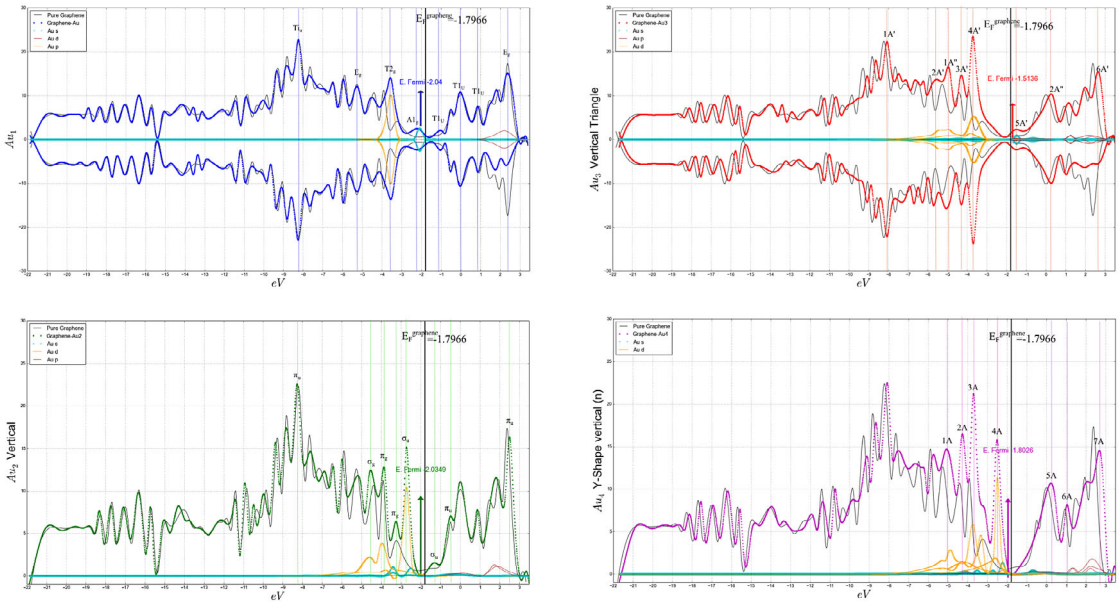

Fig. 4. DOS of graphene-Au_n system. Pure graphene (black line); the Fermi energy for pure graphene is –1.797 eV; contributions of the MOs of Au_n are indicated with dotted lines.

the graphene sheet and one gold of the trimer (gold in the apex) to the other two gold atoms (gold atoms of the triangle base), the charge transfer partially fills the 6*p* orbitals of the gold atoms.

In graphene-Au_4 system, the DOS presents an increment of density of states in the region affected directly by the tetramer. Peaks (1A), (2A) and (3A), in the occupied state region have a contribution of 5*d* orbitals of the gold tetramer and 1*p* orbital of the nearest carbons. The Fermi energy is below the Dirac point, resulting in an *n*-type doping system. The Lödwin charge analysis shows that charge transfer occurs from the graphene surface and from two gold atoms to the farthest gold atoms, resulting in the partial filling of 6*p* orbitals of gold atoms. The graphene-Au_n systems generate *n*-type doping.

Figure 5 shows the DOS of the ground state of graphene-Pt_{1-4} systems in comparison with pure graphene (black line). The electronic configuration of the platinum atom is $[Xe]\ 4f^{14}5d^{9}6s^{1}$, contributing to DOS with 5*d* and 6*s* orbitals. In graphene-Pt_1 system, the DOS has two peaks (T_{2g} and E_g), with contributions from 5*d* orbitals of platinum. The LUMO orbital is a result of the

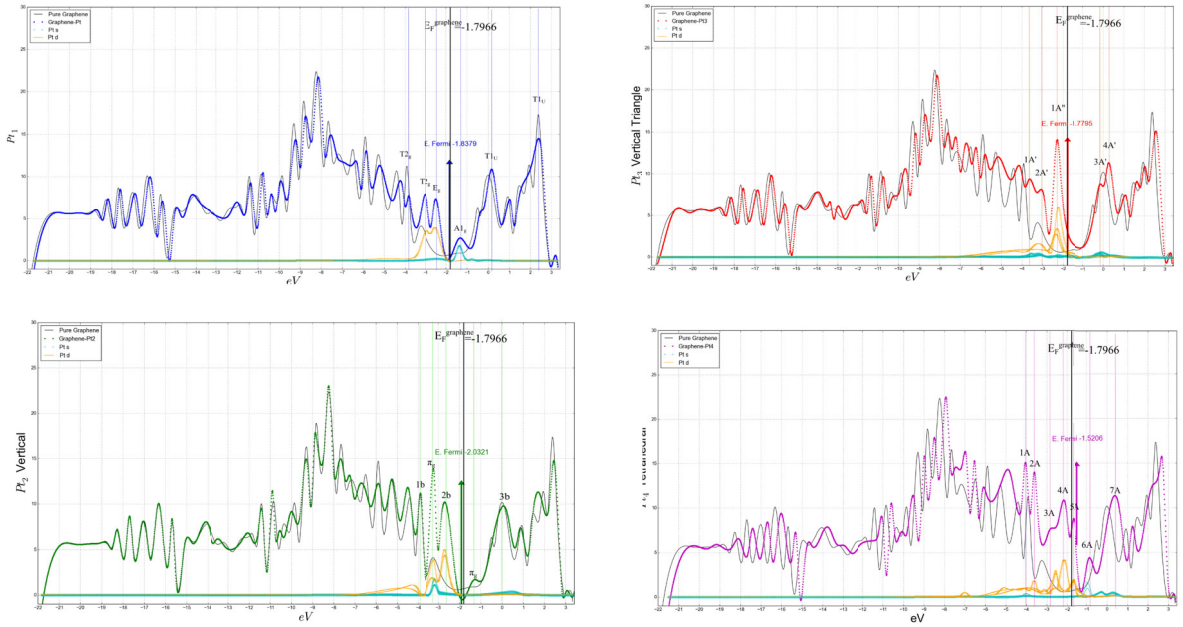

Fig. 5. DOS of graphene-Pt$_n$ system. Pure graphene (black line); the Fermi energy for pure graphene is –1.797 eV; contributions of the MOs of Pt$_n$ are indicated with dotted lines.

superposition of 6*s* orbital of platinum and 1*p* orbital of the two carbons. The Fermi energy is below the Dirac points. The Lödwin charge analysis shows that charge transfer occurs from the atom to the graphene sheet. In graphene-Pt$_2$ system, peak π_g is the superposition of 5*d* orbital and 6*s* orbital of platinum dimer, and 1*p* of carbon. The HOMO (2b) orbital is a consequence of the introduction of 5*d* states. The Lödwin charge analysis shows that the charge transfer takes place from the nearest platinum to the graphene surface, to the farthest platinum and to the graphene surface. In graphene-Pt$_3$ system, peak 2A′ consists of 6*s* orbitals from platinum trimer. The HOMO (1A″) orbital is a superposition of 5*d* and 6*s* of platinum trimer and 1*p* of graphene carbons. The Fermi energy presents a small increase in comparison to the Dirac point. The Lödwin charge analysis shows that the charge transfer takes place from the two nearest platinum atoms to the graphene surface and the farthest platinum (the apex of the triangle). In graphene-Pt$_4$ system, the DOS presents an increment of density of states in the region affected by the tetramer. Peaks 1A, 2A and 3A increase the density of states because there is an extra contribution coming from 5*d* states of the platinum tetramer. The HOMO orbital is formed by the superposition of 5*d* and 6*s* platinum atomic orbitals and 1*p* state from carbon, and crosses the Dirac point. Charge transfer comes from the cluster to the graphene sheet. The Lödwin charge analysis shows that charge transfer occurs from the 3 nearest platinum atoms to the carbon surface. The graphene-Pt$_n$ systems generate *p*-type doping.

In Figure 6, the DOS of the ground state configurations for graphene-Pd$_{1-4}$ systems in comparison with pure graphene (black line) are shown. The electronic configuration for the palladium atom is [Kr] $4d^{10}$, making a contribution to DOS with 4*s* and 4*d* orbital. In the graphene-Pd$_1$ system, the HOMO (T_{2g}) orbital receives a contribution of 4*d* orbital from the platinum atom and 1*p* orbital from carbons. LUMO (A_{1g}) is affected by 4*s* atomic orbital of palladium; the Fermi energy is below the Dirac Point. Lödwin charge analysis shows that the charge transfer is from the graphene surface to the palladium atom, partially filling the 5*p* orbital, which is depicted in the DOS as a brown line. In graphene-Pd$_2$ system, the peaks $2b_1$ and $2a_1$ are the superposition of 4*d* orbitals of palladium and 1*p* orbitals of the two nearest carbons. The difference between the Fermi energy and the Dirac point is about 0.01 eV, 4*s* orbitals only have limited influence on the LUMO orbital (p_g). Lödwin charge analysis shows that charge transfer occurs from the graphene sheet to the palladium atom, partially filling the 5*p* orbital. In graphene-Pd$_3$ system, the HOMO (2A′) has contributions from 4*d* orbitals of the palladium trimer, 1*p* orbitals from the 3 nearest carbons and a small contribution of 4*s* orbitals from palladium atoms. Lödwin charge analysis shows that the charge transfer takes place from the graphene sheet towards the palladium trimer, partially filling 5*p* orbitals of palladium atoms. Fermi energy exceeds the Dirac point, suggesting that the charge transfer is from the trimer to the graphene sheet. In graphene-Pd$_4$ system, the DOS presents an increase in the HOMO (4A) orbital due to the presence of 4*d* orbitals of palladium atoms and 1*p* orbitals from the four nearest carbons. The LUMO (5A) also has an increase of density of states, in comparison with pure graphene. The Fermi energy exceeds the Dirac Point. The Lödwin charge analysis shows that charge transfer occurs from the graphene surface and one palladium atom (tetrahedral apex), to the other three palladium atoms (tetrahedral basis). The graphene-Pd$_n$ systems show *n*-type doping.

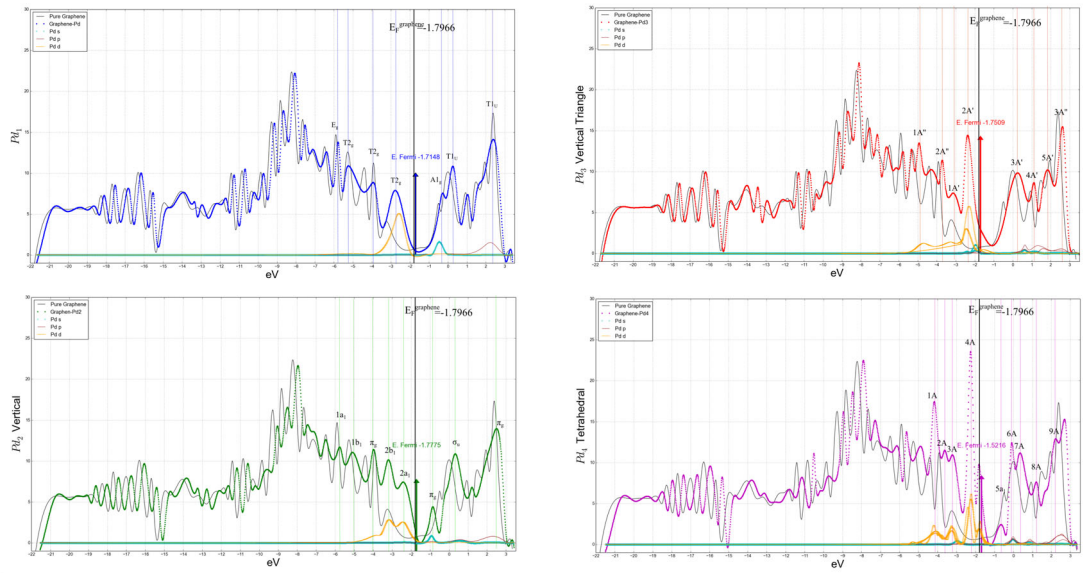

Fig. 6. DOS of graphene-Pd$_n$ system. Pure graphene (black line); the Fermi energy for pure graphene is –1.797 eV; contributions of the MOs of Pd$_n$ are indicated with dotted lines.

3.3 Conductivity

We are interested in studying how clustering of adsorbates attached to the graphene surface can influence electrical conductivity. As we mentioned in the introduction, there are three ways to predict conductivity on graphene. In this paper, we study conductivity, by applying the Frozen Ripples Approach (FRA), Charged Impurities Scattering Approach (CISA) and Resonant Scattering Approach (RSA).

In FRA, the focus proposed considers the effect of deformation on the surface of graphene, in connection with electrical conductivity. Katsnelson and Geim showed that the scattering of electrons, short-range potential, is likely to be controlled by charged impurities and ripples (microscopic corrugations of a graphene sheet) [10]. They also show, that certain types of ripples create a long-range scattering potential, similar to Coulomb scatters, and result in charge-carrier mobility, practically independent of carrier concentration. The electrons in graphene are dispersed by the graphene curvature, due to a potential that is proportional to the square of the local curvature. If electrons are scattered, we may assume that resistivity increases, moving away from pure graphene ballistic behaviour. Katsnelson and Geim approximated the excess resistivity as:

$$\delta\rho \approx \frac{h}{4e^2}\frac{z^4}{R^2a^2},$$

where z and R are the characteristic height and radius of ripples, respectively.

In a paper published by Katsnelson et al. in 2009 [11], they analysed the scattering of Dirac fermions by clusters of charged impurities (CISA) and showed that at this doping level, this disorder results in significantly higher conductivity. Moreover, for a fixed amount of impurities, the formation of large circular clusters will decrease the scattering cross section, compared to that of isolated single atoms [34]. This would manifest itself experimentally as an increase in mobility, observed in the experiments under cryogenic [14,35,36] and ambient [12] conditions. Likewise, a sharp increase in resistivity, observed above 200 K is not anticipated with traditional theory, but with frozen ripples can be qualitatively understood. There are two regimes; $k_FR \ll 1$, where the cluster is small compared to the Fermi wavelength, thus weakly perturbing the electronic wave function; and the adiabatic approximation can be used to obtain a constant expression for $\sigma_{tr} \propto k_FR^2\,(\frac{V}{\hbar v_F R^{-1}})^2$; $k_FR \gg 1$, the cross section is a function of the incident angle q and the total cross section (angular resolved and the integrated cross section) show resonances associated with quasibound states inside the cluster. They estimate conductivity (g) as a function of Fermi wavelength (k_F), the square of the potential (V), the Fermi velocity (v_F), the cluster concentration density (n_c), and the distortion radius (R) to the fourth power.

$$g = \frac{e^2}{h}k_Fl \sim \begin{cases} \frac{e^2}{h}\frac{1}{n_cR^2}\left(\frac{\hbar v_F R^{-1}}{V}\right)^2, & k_FR \ll 1 \\ \frac{e^2}{h}\frac{k_F^2}{n_c}, & k_FR \gg 1. \end{cases}$$

In this model, it is most important to express conductivity in terms of cluster concentration density (n_c) and not in terms of carrier concentration. Another fact used in this approach, is that if disorder inside the cluster is weak, the local mean-free path (l) exceeds the electron wavelength inside the cluster $\lambda \approx \hbar v_F/V$. If disordered is stronger than the local mean-free path, we can reach the Mott limit $l \approx \lambda$ due to Klein tunnelling [37]. The potential V describes the shift in chemical potential due to adsorbates; we used V to represent adsorption energies.

In RSA, the semiclassical Boltzmann theory is used to calculate conductivity as a function of carrier density.

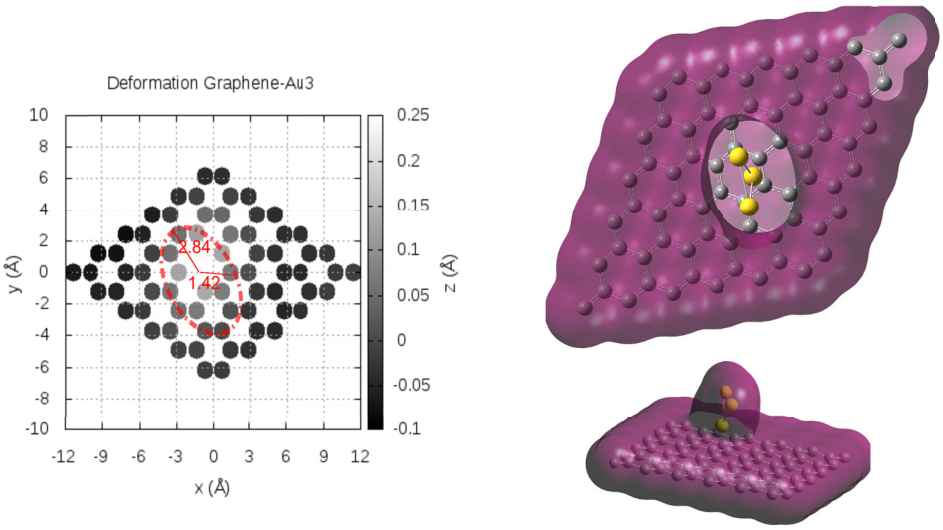

Fig. 7. Deformation of graphene with gold clusters (graphene-Au_3). The CDS surface is also shown.

An additional scattering mechanism has been proposed involving midgap states [38], leading to a similar k dependence of the relaxation time as charged impurities. The midgap state mechanism can be interpreted as boundaries, cracks, adsorbates or vacancies, and induced a high potential difference with respect to the graphene sheet [39,40]. Consequently, the phase shift must approach zero for wave vectors close to the Dirac point. For a short-range contact potential, the phase shift's behaviour is not linear but logarithmic [41–45]. In some cases, adsorbates on graphene can give resonance that is fairly close to the point of neutrality [46]. Using Boltzmann equation, conductivity can be estimated by the T matrix

$$g \approx \left(\frac{2e^2}{h}\right)\left(2\pi n_i \left|\frac{T(E_F)}{D}\right|^2\right)^{-1},$$

with $D = \sqrt{\sqrt{3}\pi t}$ and t is the nearest-neighbour hopping parameter. In the limit of resonant impurities, conductivity is [12]

$$g \approx \left(\frac{4e^2}{\pi h}\right)\frac{n_e}{n_i}\ln^2\left|\frac{E_F}{D}\right|,$$

where $n_e = E_F^2/D^2$ is the number of charge carriers per carbon atom. The effective impurity radius is $R = \hbar v_F/D$; we calculate D in terms of R and v_F. The Boltzmann approach becomes questionable at high purity concentrations, and does not work near the neutrality point, where quantum corrections are dominant [11,43–45]. However for small clusters, this may be sufficient to qualitatively predict conductivity behaviour in graphene-M_n systems.

Using these conductivity models and $v_F = \sqrt{2E_F/m_e}$, we estimate the conductivity of the graphene sheets, with the adsorption of the metallic clusters. We also used two criteria to obtain the deformation parameter R. The first one requires considering only the optimised graphene layer having in interaction with the metallic clusters. Graphene deformations were plotted in terms of their atomic coordinates, radius and heights. The heights above the plane are shown in grey scales and consider the z coordinate in the plane of the centre of mass (see Fig. 7). Deformation radiuses are taken as the distance between the maximum and the minimum height, near to the adsorbate. The criteria outlined above provide the most direct method for considering the deformation radius. On the other hand, the charge density surface (CDS) shows how the adsorption of metal clusters in graphene is responsible for electron scattering in the transport phenomenon. The CDS directly shows the area where electrons are dispersed, providing us with information about the potential at which electrons are scattered and indicates the deformation radius. The CDS is another method for measuring the radius of deformation. We compare both criteria to get the best measurement of the radii. Deformation is in the area closest to the metal cluster with its centre near the metal. In some cases, deformation is diagonal and forms an ellipse, as follows from reference [46] in which a scattering theory for bilayer graphene with a cylindrical potential well of radius R is developed, the radius of deformation was taken as the average of minor and major radii (see Fig. 7).

Table 3 shows all parameters involved in the calculation of conductivity. The $k_F R$ parameter reaches the value $k_F R \approx (1.6\text{–}3.05) \times 10^{-19} \ll 1$ for 1.4 Å $\leq R \leq$ 2.7 Å. The cluster concentration n_c was calculated with the unit cell's parameters and was around 2.9×10^{13} cm^2.

Our results fall within the range of some experimental results; Pasricha et al. [47] made an experimental study where they measured the electrical conductivity of Ag-graphene-based nanocomposites. In particular, they present graphene-Ag nanosheets after a reduction of Ag-graphite oxide, with an average size of a single layer of 150–250 nm and a height of 1.2–1.5 nm. Electrical conductivity measured by Pasricha et al. was of 155 S cm^{-1}. Sundaram et al. [48] used the fact that relative low contact resistance is around 340 W mm and measured an electrical conductivity of 294 S cm^{-1}, attesting to the quality of the graphene-gold interface.

Table 3. Conductivities and parameter used for the calculation. Fermi energy (E_F) in eV, radius of deformation (R) in Å, height (z) in Å, v_F in (m/s), shift in chemical potential (V) in eV, and conductivity (g) in S/cm.

System	FRA				CISA			RSA		
	E_F [eV]	R [Å]	z [Å]	g [S/cm]	v_F [m/s]	V [eV]	g [S/cm]	$D(R)$ [eV]	n_e/ C-atom	g [S/cm]
Graphene-Ag	–1.72	1.43	0.025	148.78	7.77×10^5	0.03	128.53	1.89	0.82	153.27
Graphene-Ag_2	–1.70	2.46	0.03	23.34	7.73×10^5	0.13	60.73	2.06	0.67	47.94
Graphene-Ag_3	–1.06	2.66	0.163	6.03	6.09×10^5	0.36	3.60	1.51	0.49	14.18
Graphene-Ag_4	–1.25	3.36	0.073	1.24	6.64×10^5	0.3	2.49	1.30	0.93	21.32
Graphene-Au	–2.04	1.43	0.020	34.11	8.47×10^5	0.31	40.77	3.90	0.27	33.24
Graphene-Au_2	–2.04	1.42	0.12	12.16	8.46×10^5	0.64	27.05	3.92	0.27	15.63
Graphene-Au_3	–1.51	2.13	0.25	0.36	7.30×10^5	0.75	2.89	2.25	0.45	8.83
Graphene-Au_4	–1.80	2.65	0.061	1.63	7.96×10^5	0.66	1.86	1.98	0.83	13.00
Graphene-Pt	–1.84	1.94	0.33	0.15	8.04×10^5	1.2	1.99	2.73	0.45	6.09
Graphene-Pt_2	–2.03	1.98	0.12	6.78	8.45×10^5	0.94	3.32	2.81	0.52	9.67
Graphene-Pt_3	–1.78	2.39	0.21	1.27	7.91×10^5	1.82	0.37	2.18	0.67	3.23
Graphene-Pt_4	–1.52	2.65	0.33	0.19	7.31×10^5	1.27	0.42	1.82	0.70	4.32
Graphene-Pd	–1.72	1.94	0.25	1.04	7.77×10^5	1.2	1.86	2.64	0.42	5.54
Graphene-Pd_2	–1.53	2.52	0.12	9.93	7.35×10^5	1.35	4.62	1.92	0.64	4.01
Graphene-Pd_3	–1.76	2.27	0.21	1.27	7.85×10^5	1.98	3.75	2.28	0.59	2.79
Graphene-Pd_4	–1.52	2.66	0.145	3.21	7.30×10^5	0.61	1.88	1.81	0.70	1.55

It is first notable that all three approaches present similar results and trends. The Ag and Au systems show a decrease in conductivity as the size of the cluster increases, whereas for Pt and Pd systems the single atom manifests less conductivity than the dimer, Figure 8. The latter is probably due to a stronger interaction between a single atom and the graphene, than between the dimer and the graphene. Silver system shows the least deformation and the highest conductivity, whereas Pt and Pd systems show the lowest conductivities. This is due to the fact that silver and gold are physisorbed, whereas platinum and palladium are chemisorbed and thus the interaction with the system is stronger.

Comparing DOS with electronic conductivity, apparently conductivity behaves according to the DOS. In the DOS, it is evident that occupied s states from the metal have the essential effect in terms of electronic conductivity. In graphene-Ag_1, the s states from Ag are at the Fermi energy, increasing electronic conductivity. Meanwhile, in graphene-Au_1, s states are near the Fermi energy (in HOMO region) but there are only a few states in LUMO region, so electron transport is limited. Generally, incrementing the metallic atoms increases the number of s states, but the s states appear in regions that do not favour electronic conductivity (far from the Fermi energy). For this reason, there is no improvement in conductivity when the s states increase in number or when the number of metallic atomsare increased; the interaction between the surface and metal is stronger than the interaction between the metals. Observing all this, it can be deduced that a big Ag cluster could increase the number of states, such that there are s states in the Fermi region to increase conductivity.

For FRA, apparently increasing the number of atoms causes the size of radius to decrease. Systems graphene-Ag_n, graphene-Au_n and graphene-Pt_n appear to diminish the conductivity. Meanwhile, the graphene-Pd_n system cannot be well-described with this approach, in as much as the deformation increases, the conductivity dramatically decreases and the model is no longer appropriate. For CISA, conductivity clearly depends on adsorption energies; the graphene-Pd_n is analogous. Applying either approach, the network is distorted, breaking the natural two-dimensionality of the graphene sheet and enhancing the size of the scattering centre. With an increase in the scattering centre's size, the electron mean-free path l notoriously decreases and electrical conductivity ceases to be in the ballistic regimen. In RSA, hybridization gives place to a shift in the effective resonance level up to the Dirac point, which is also a consequence of level repulsion that pushes additional states towards the region with the lowest density of states. Thus, systems that are better described by RSA are those that manifest a substantial increment in the density of states in the Fermi region.

4 Conclusions

The studied structures show that graphene-Ag_n and graphene-Au_n systems fall within the physisorption range; meanwhile graphene-Pt_n and graphene-Pd_n are in the chemisorption range. In these cases, bond-lengths indicate that the interaction between two metallic atoms (M-M) is stronger than the interaction between graphene and a metallic atom (M-C).

The DOS and charge transfer analysis shows that in graphene-Ag systems and graphene-Pt systems, the charge is transferred from the metallic atoms to graphene sheets (p-doping). In the case of graphene-Au_n and graphene-Pd_n systems, the charge flows from the graphene sheets to the metallic cluster (n-doping). The localized nature of the charge changes electronic mobility and scattering is predominant over the increase or decrease of charge

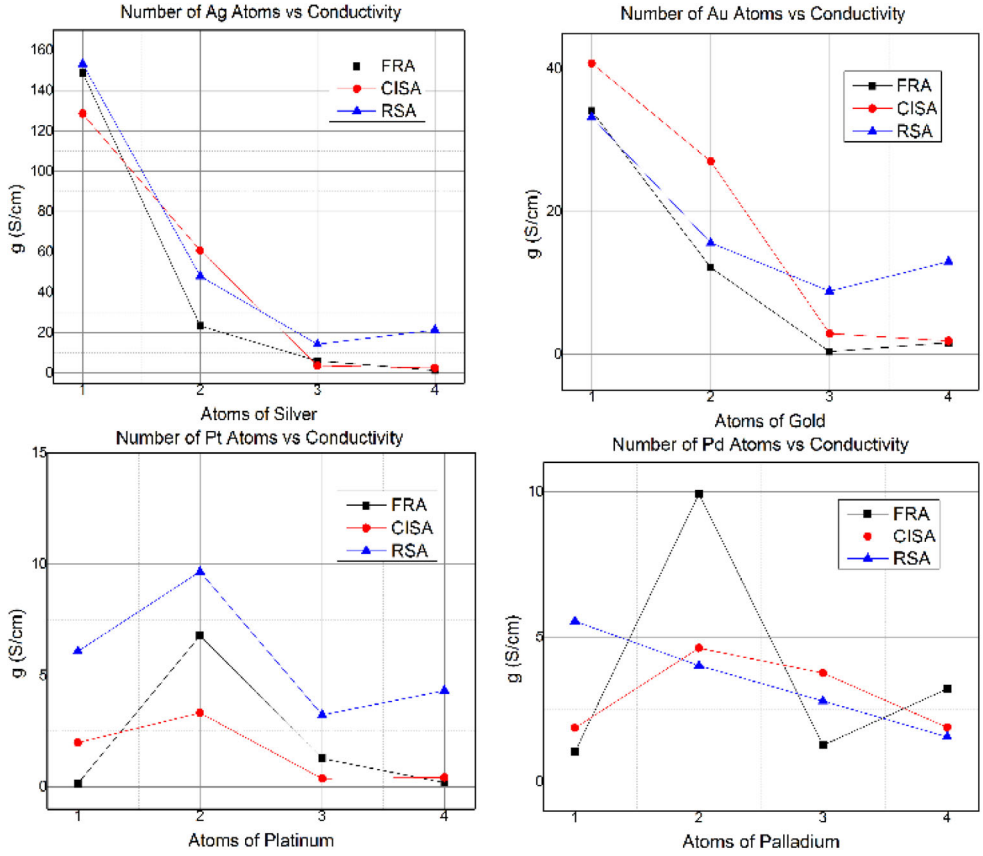

Fig. 8. Conductivity as a function of number of atoms in the cluster.

carriers. The DOS analysis allows us better comprehend the connection between adsorption and conductivity. For *p*-doping systems, the metallic atom makes a contribution with its *s* and *d* valence orbital. For *n*-doping systems, the explicit contribution is present from the *s*, *p* and *d* valence orbitals of the metallic atom.

The presence of extremely small metallic clusters on the graphene sheets deformed the π-π network of graphene, inducing a loss of electrical conductivity. The trend in conductivity shows that as the adsorption energy of the system increases, the network distorts breaking the natural two-dimensionality of the graphene sheet and enhancing the size of the scattering centre (height). With increasing scattering centre size, the electron mean-free path l notoriously decreases and electrical conductivity leaves the ballistic regimen. The best system for conserving ballistic conductivity is the graphene-Ag_n, which is in the physisorption range for all clusters studied.

Author contribution statement

All authors contributed equally to the paper.

We would like to thank CONACYT for Roxana del Castillo's scholarship and DGTIC UNAM for the Supercomputing facilities and technical assistance.

References

1. K.S. Novoselov, A.K. Geim, S.V. Morozov, D. Jiang, Y. Zhang, S.V. Dubonos, I.V. Grigorieva, A.A. Firsov, Science **306**, 666 (2006)
2. S. Bae, H. Kim, Y. Lee, X. Xu, J. Park, Y. Zheng, J. Balakrishnan, T. Lei, H. Kim, Y. Song, Y. Kim, K.S. Kim, B. Özyilmaz, J. Ahn, B. Hong, S. Iijima, Nat. Nanotechnol. **5**, 574 (2010)
3. J.S. Wang, Y. Geng, Q. Zheng, J. Kim, Carbon **48**, 1815 (2010)
4. S.L. Hellstrom, H.W. Lee, Z. Bao, ACS Nano **23**, 1423 (2009)
5. H. Chen, Z. Gao, Y. Cui, G. Chen, D. Tang, Biosensors Bioelectronics **44**, 108 (2013)
6. E.L. Ratcliff, P.A. Lee, N.R. Armstrong, J. Mater. Chem. **20**, 2672 (2010)
7. B. Partoens, F.M. Peeters, Phys. Rev. B **74**, 075404 (2006)
8. A.K. Geim, K.S. Novoselov, Nat. Mater. **6**, 183 (2007)
9. T. Ando, J. Phys. Soc. Jpn **75**, 074716 (2006)
10. M.I. Katsnelson, A.K. Geim, Phil. Trans. R. Soc. A **366**, 195 (2008)
11. M.I. Katsnelson, F. Guinea, A.K. Geim, Phys. Rev. B **79**, 195426 (2009)
12. T.O. Wehling, S. Yuan, A.I. Lichtenstein, A.K. Geim, M.I. Katsnelson, Phys. Rev. Lett. **105**, 056802 (2010)
13. F. Schedin, A.K. Geim, S.V. Morozov, E.W. Hill, P. Blake, M.I. Katsnelson, K.S. Novoselov, Nat. Mater **6**, 652 (2007)
14. M. Caragiu, S. Finberg, J. Phys.: Condens. Matter **17**, R995 (2005)

15. K.M. Mc Creary, K. Pi, A.G. Swartz, H. Wei, W. Bao, C.N. Lu, F. Guinea, M.I. Katsnelson, R.K. Kawakami, Phys. Rev. B **81**, 115453 (2010)
16. H.W. Tien, Y. Huang, S. Yang, J. Wang, C.M. Ma, Carbon **49**, 1550 (2011)
17. M. Vanin, J.J. Mortensen, A.K. Kelkkanen, J.M. Garcia-Lastra, K.S. Thygesen, K.W. Jacobsen, Phys. Rev. B **81**, 081408(R) (2010)
18. M. Amft, B. Sahyal, O. Eriksson, N. Skorodumova, J. Phys.: Condens. Matter **23**, 395001 (2011)
19. I. Cabria, M.J. López, A. Alonso, Phys. Rev. B **81**, 035403 (2010)
20. P. Giannozzi et al., J. Phys.: Condens. Matter **21**, 395502 (2009)
21. J.P. Perdew, K. Burke, M. Ernzerhof, Phys. Rev. Lett. **77**, 3865 (1995)
22. M. Methfessel, A.T. Paxton, Phys. Rev. B **40**, 3616 (1989)
23. H.J. Monkhorst, J.D. Pack, Phys. Rev. B **13**, 5188 (1976)
24. D. Vanderbilt, Phys. Rev. B **41**, 7892 (1990)
25. A.M. Rappe, K.M. Rabe, E. Kaxiras, J.D. Joannopoulos, Phys. Rev. B **41**, 1227 (1990); Erratum, Phys. Rev. B **44**, 13175 (1991)
26. K. Okazaki-Maeda, Y. Morikawa, M. Tanaka, S. Kohyama, Surf. Sci. **604**, 144 (2010)
27. H. Grönbeck, W. Andreoni, Chem. Phys. **262**, 1 (2000)
28. H. Hakkinen, B. Yoon, U. Landman, X. Li, H.-J. Zhai, Lai Wang, J. Phys. Chem. A **32**, 6168 (2003)
29. R. Thapa, D. Sen, M.K. Mitram, K.K. Chattopadhyay, Physica B **406**, 368 (2011)
30. S. Lin, B. Strauss, A. Kant, J. Chem. Phys. **51**, 2282 (1969)
31. O. Leenaerts, B. Paertoens, F.M. Peeters, Phys. Rev. B **77**, 125416 (2008)
32. P.O. Löwdin, Adv. Quantum Chem. **5**, 185 (1970)
33. L. Van Hove, Phys. Rev. B **89**, 1189 (1953)
34. F. Guinea, J. Low Temp. Phys. **153**, 356 (2008)
35. J.H. Chen, C. Jang, S. Adam, M.S. Fuhrer, E.D. Williams, M. Ishigami, Nat. Phys. **4**, 377 (2008)
36. S.V. Morozov, K.S. Novoselov, M.I. Katsnelson, F. Schedin, D.C. Elias, J.A. Jaszczk, A.K. Geim, Phys. Rev. Lett. **100**, 016602 (2008)
37. M.I. Katsnelson, K.S. Novoselov, A.K. Geim, Nat. Phys. **2**, 620 (2006)
38. T. Stauber, N.M.R. Peres, F. Guinea, Phys. Rev. B **76**, 205423 (2007)
39. M. Fujita, K. Wajabayashi, K. Nakada, K. Kusakabe, J. Phys. Soc. Jpn **65**, 1920 (1996)
40. M.A.H. Vozmediano, M.P. López-Sancho, T. Stauber, F. Guinea, Phys. Rev. B. **72**, 155 (2005)
41. M. Hentschel, F. Guinea, Phys. Rev. B. **76**, 115407 (2007)
42. M.I. Katsnelson, K.S. Novoselov, Solid State Commun. **143**, 3 (2007)
43. P.M. Ostrovsky, I.V. Gornyi, A.D. Mirlin, Phys. Rev. B **74**, 235443 (2006)
44. M.I. Katsnelson, Eur. Phys. J. B **51**, 157 (2006)
45. M. Auslender, M.I. Katsnelson, Phys. Rev. B **76**, 235425 (2007)
46. M.I. Katsnelson, Phys. Rev. B **76**, 073411 (2007)
47. R. Pasricha, S. Gupta, A.K. Srivastava, Small **20**, 2253 (2009)
48. R.S. Sundaram, M. Steiner, Chiu Hsin-Ying, M. Engel, A.A. Bol, R. Krupke, M. Burghard, K. Kern, P. Avouris, Nano Lett. **11**, 3833 (2011)